Bioprinting 31 (2023) e00270

Contents lists available at ScienceDirect

Bioprinting

journal homepage: www.sciencedirect.com/journal/bioprinting

3D bioprinting of gene delivery scaffolds with controlled release

Yi Xiang [a], Zheng Zhong [a], Emmie J. Yao [a], Wisarut Kiratitanaporn [b], Malleeka T. Suy [c], Shaochen Chen [a,b,*]

[a] Department of NanoEngineering, University of California, San Diego, La Jolla, CA, 92093, USA
[b] Department of Bioengineering, University of California, San Diego, La Jolla, CA, 92093, USA
[c] Department of Biological Science, University of California, San Diego, La Jolla, CA, 92093, USA

ARTICLE INFO

Keywords:
3D bioprinting
Gene delivery
Scaffold
Hydrogel

ABSTRACT

Localized gene delivery via engineered scaffolds offers spatiotemporal control of the gene vector release. Here, we explored the capability of digital light processing based bioprinting to fabricate 3D scaffolds in hydrogels for controlled gene delivery. We demonstrated the compatibility of the method with three representative hydrogel biomaterials for gene delivery. We further investigated the highly tunable release profile with these scaffolds by creating and combining distinct release mechanisms of diffusion and ion exchange. The efficacy of gene delivery of these scaffolds was validated *in vitro* using 293T cells. Results from this work could potentially facilitate the development of synergistic and personalized gene therapies.

1. Introduction

The past few decades have seen the emergence of gene therapy as a durable and curative treatment, especially for intractable diseases such as hemophilia, neurodegenerative disorders, blindness, and hypercholesterolemia [1,2], as well as for tissue regeneration, for example, adenoviral vector-mediated gene therapies have been validated for stable and improved cartilage repair in large animals over a long period [3]. The efficiency of gene therapy has been further improved by application of local delivery, by which the vectors could be enriched in the target organ and side events at other sites of the body could potentially be bypassed [4]. Engineered scaffolds have been developed and utilized to facilitate the local delivery of the gene therapy agents due to their capacity to load therapeutic level of the vectors in a single dose and mediate the administration of the vectors temporally and spatially. For example, Ho et al. used mesenchymal stem cell membrane-coated poly (ε-caprolactone) nanofibril scaffold fabricated by electrospinning to enhance the targeted and sustained delivery of CRISPR/Cas9 toward the Leukemia stem cells, achieving an extended *in vivo* retention time and reduced cytotoxicity [5]. Moreover, 3D organization of the scaffold holds the potential to support cell growth and guide them into functional tissue, as well as protection of vector integrity [6].

The advancement and translation of gene therapy concur with the development of the fabrication techniques of the scaffold. As an advanced additive manufacturing technique, digital light projection (DLP)-based 3D printing offers a rapid and highly customized capability for the fabrication of tissue engineering scaffolds. In the DLP printing system, a digital micromirror device, which is an array of millions of micromirrors, reflects the projected light in a user-defined pattern onto a photopolymerizable material reservoir to create a designated construct [7] (Fig. 1C). The DLP printing technique is compatible with a variety of biomaterials which have been demonstrated as a gene delivery implant, such as gelatin methacrylate (GelMA) [8], hyaluronic acid glycidyl methacrylate (HAGM) [9], chitosan methacrylate (ChiMA) [10], and alginate methacrylate (AlgiMA) [11]. With the user-defined patterns, multiple forms of scaffolds could be printed via DLP, such as log-piles [12], conduits [13], and injectable microparticles [14], allowing for personalized treatment.

In addition to the spatial control administered by the form of scaffold, distinct release rates of the gene cargoes are desired in different applications. The sustained release of transient expression vectors is desired in many clinical applications because it maintains a constant level of target protein expression with no risk to the genomic integrity of the recipient [15].The release rate of the gene cargoes could be modulated based on the diffusion and degradation kinetics of the substrate material, which could be regulated in the DLP printing system by tuning the printing parameters including light intensity and exposure time to control the pore size and degree of polymerization of the material. In addition to the essential regulating role of the diffusion and degradation, the release kinetics could also be effectively tuned by the electrostatic

* Corresponding author. Department of NanoEngineering, University of California, San Diego, La Jolla, CA, 92093, USA.
E-mail address: shc064@ucsd.edu (S. Chen).

https://doi.org/10.1016/j.bprint.2023.e00270
Received 7 January 2023; Received in revised form 28 February 2023; Accepted 20 March 2023
Available online 21 March 2023

adsorption. Electrostatic adsorption occurs between the particles and the substrate with opposite charges that are firmly stabilized by the Coulomb's force. In this case, the particles are sustainedly released by ion exchange, external forces, and material degradation before diffusing out of the scaffold [16]. In contrast, when the particles are loaded in the substrate which has the same charge as itself, the electrostatic repulsion could drive and accelerate the diffusion process [17]. With a wide range of material compatibility, proper coupling of the gene delivery cargo and the choice of material holds the potential to enable further regulation on the release kinetics.

In this study, we present a novel approach for scaffold-mediated gene therapy using a DLP printing platform. We investigate the use of three different materials, AlgiMA, ChiMA, and GelMA, each with different electrical charges, as scaffolds to mediate the ion exchange-based release of gene delivery cargoes. We hypothesize that compared to the release mediated by diffusion solely, the electrostatic adsorption could allow for a more tailored release kinetic of the gene vector with a wider tunable range. To validate this hypothesis, scaffolds of each material were printed by encapsulating two typical types of gene cargo, adeno-associated virus type 2 (AAV-2) and lipofectamine 3000, respectively. The release profiles of the two cargoes in each material were investigated and compared, and the functionality of the DLP printed scaffold was tested. This is the first use of the DLP printing platform for scaffold-mediated gene therapy. This work can potentially lead to more effective treatments in the future.

2. Material and methods

2.1. GelMA synthesis

GelMA was synthesized from type A gelatin (Cat. #G2500, Sigma-Aldrich) and methacrylic anhydride (MA, Cat. # 276685, Sigma Aldrich) in a 0.25 M carbonate-bicarbonate (CB) buffer as previously described [18]. Briefly, a 10%(w/v) gelatin solution in the CB buffer was allowed to react with MA at a MA/gelatin ratio of 0.085 mL/g for 1 h at 50 °C. The reaction was then quenched by adjusting the pH to 7.4. The reactant was subsequently dialyzed in 12–14 kDa cutoff dialysis tubings (Cat. # 132706, Spectrum Labs) against MilliQ water for 3 days and lyophilized for future use.

2.2. AlgiMA synthesis

The protocol for AlgiMA synthesis was adapted from a previous publication [19]. Briefly, 1%(w/v) sodium alginate (Cat. #A1112, Sigma Aldrich) solution was prepared in a MES buffer containing 0.5 M NaCl (Cat. #S671, Fisher) and 50 mM 2-morpholinoethanesulfonic acid (MES, Cat.#M0606, TCI) with a pH of 6.5. The carboxyl groups of the alginate were activated with N-hydroxysuccinimide (NHS, Cat. # 130672, Sigma Aldrich) and 1-ethyl-3-(3-dimethylaminopropyl)-carbodiimide hydrochloride (EDC, Cat. #341006, Sigma Aldrich) for 5 min 2-Aminoethyl methacrylate hydrochloride (AEMA, Cat. # AC357810250, Acros Organics) was added to the reaction subsequently and reacted for 24 h. The molar ratio of the reagents was set at NHS: EDC: AEMA = 1:2:1, and AEMA was added by 2.3 mmol per gram sodium alginate. The reaction was quenched by precipitating the reactant with excess amount of acetone. The precipitation was then dissolved in MilliQ water and dialyzed against MilliQ water in 12–14 kDa cutoff dialysis tubings for 3 days before lyophilized for storage. All the synthesis and purification procedures were performed at room temperature.

2.3. ChiMA synthesis

ChiMA was synthesized adapting the protocol reported by Yu et al. [20]. Chitosan (Cat. #50494, Sigma Aldrich) was dissolved in 2%(w/w) acetic acid (Cat.# 320099, Sigma Aldrich) to obtain a 3%(w/v) solution. Methacrylic anhydride (Cat. # 276685, Sigma Aldrich) was added dropwise by 0.4 M per chitosan repeating unit at 60 °C for 3 h. The reactant was then dialyzed against MilliQ water in 12–14 kDa cutoff dialysis tubings for 3 days and lyophilized.

2.4. LAP synthesis

Lithium phenyl-2,4,6-trimethylbenzoylphosphinate (LAP) was synthesized per the protocol previously published [21]. Briefly, 2,4,6-trimethylbenzoyl chloride (Cat. #C965Y83, Thomas Scientific) and dimethyl phenylphosphonite (Cat. # 149470, Sigma-Aldrich) was combined to react for 18 h under argon flow to produce the intermediate compound phenyl-2,4,6-trimethylbenzoyl phosphite. The intermediate was then reacted with a lithium bromide (Cat. # 213225, Sigma-Aldrich) solution in 2-butanone (Cat. #M209-4, Thermo Fisher Scientific) for 10 min at

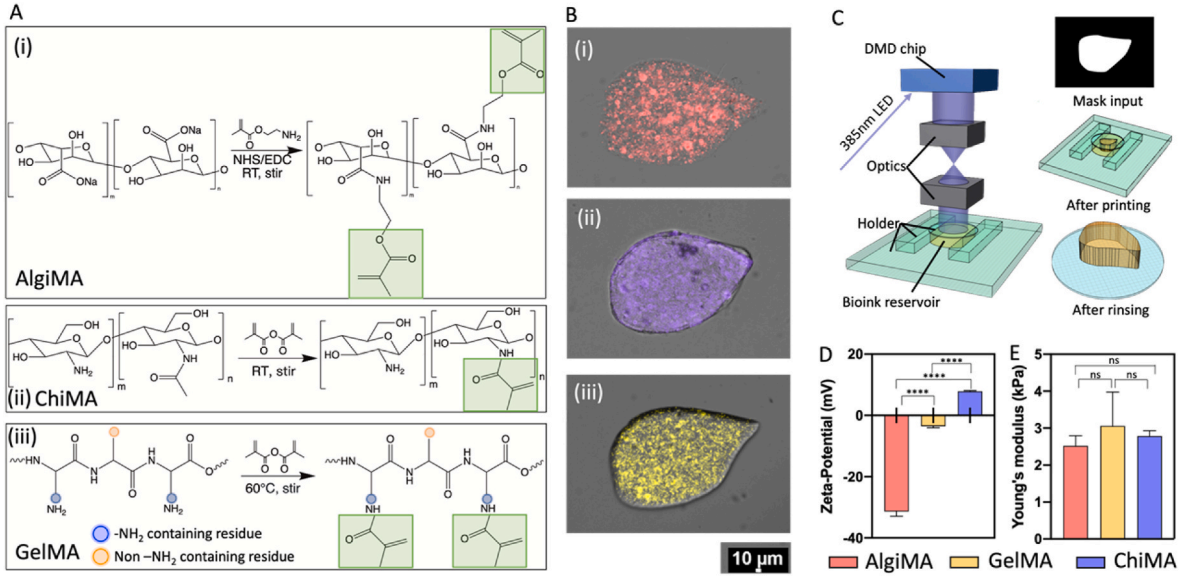

Fig. 1. A. Synthesis of AlgiMA, ChiMA and GelMA; B. Printing examples of (i) AlgiMA, (ii) ChiMA and (iii) GelMA scaffolds with resolved micro-scale features; C. illustration of DLP printing; D. Distinct zeta-potential of AlgiMA, GelMA and ChiMA ($P < 0.0001$****); E. Similar Young's modulus of AlgiMA, GelMA and ChiMA at the chosen concentration (AlgiMA vs. GelMA: $P = 0.146$; AlgiMA vs. ChiMA: $P = 0.2322$; GelMA vs. ChiMA: $P = 0.2076$).

50 °C. The reaction was then equilibrated to room temperature, and the reactant was precipitated and washed with excessive 2-butanone. The product was air-dried overnight and stored under argon at 4 °C.

2.5. Coverslip methacrylation

Glass coverslips were grafted with methacrylate to create a robust binding between the coverslip and the scaffolds after DLP printing. Briefly, glass coverslips were cleaned with ethanol (Cat. # 71002-426, VWR) and incubated in a solution consisting of 1.75%(v/v) 3-(Trimethoxysilyl)-Propyl Methacrylate (TMSPMA) (Cat. #M6514-50 ML, Sigma-Aldrich), 10.50%(v/v) 1:10 acetic acid: ethanol, and 87.75%(v/v) 100% ethanol overnight on a shaker at room temperature. The reagents were then removed by washing twice with ethanol and washing twice with MilliQ water before air-dried for storage.

2.6. Bioink preparation

AlgiMA, ChiMA, GelMA and LAP were dissolved in Dulbecco's phosphate-buffered saline (DPBS, Cat. # 14190144, Gibco) to create a stock solution of 4%(w/v), 4%(w/v), 20%(w/v) and 4%(w/v), respectively. The GFP expression plasmid (pLenti-CMV-GFP-Puro) was a kind gift from Dr. Liangfang Zhang's group at the University of California San Diego. Lipofectamine3000 (Cat. #L3000001, Invitrogen) was prepared per the manufacture's recommendations with Opti-MEM (Cat. #31985070, Gibco) and the product was added as 20%(v/v) of the final bioink. AAV-2 (pAAV-CAG-GFP) was acquired from Dr. Edward Boyden (Addgene # 37825; http://n2t.net/addgene:37825; RRID:Addgene_37825) and was added to the bioink to a final concentration of 2×10^{12} GC/mL. In all samples, LAP was added to reach a final concentration of 0.6%(w/v). Each component was combined at the designated ratio and mixed by pipetting right before printing.

2.7. DLP printing

DLP printing was performed with an in-house built printer [14] facilitated by holder, which was a stack of polydimethylsiloxane (PDMS) sheets. The bioink was added to the gap between the holder and the coverslip to form a reservoir. The height of the sample was thus controlled by the thickness of the PDMS sheets (Fig. 1C). A 385 nm LED light with user defined pattern illuminates the reservoir to polymerize the designated area. For the printing resolution test, masks shown in Figs. S1 and 250 μm PDMS sheets were used. For all the release and functionality test samples, a 3×3 mm^2 square mask and 1 mm PDMS sheets were used to create slab scaffolds with a final volume of 9 μL. For mechanical testing, a circle mask with a diameter of 1.5 mm and 1 mm PDMS sheets were used to create pillar samples. For scanning electron microscopy (SEM) imaging of the scaffold surface, a 1×1mm^2 square mask and 250 μm PDMS sheets were used to create the slab specimens.

2.8. Scanning electron microscopy (SEM)

The specimens were lyophilized prior to SEM imaging. The specimens were then affixed to the imaging stage using carbon tape and sputter coated with iridium using Emitech K575X sputter coater. The imaging was conducted with Zeiss Sigma 500 at 3 kV.

2.9. Mechanical testing

A commercially available Microsquisher tester (Cellscale) was used for mechanical testing. The experiment was performed per the manufacture's manual. The samples were compressed at 10% strain with a 2 μm/s strain rate, and the Young's modulus was calculated based on the collected data with an in-house developed MATLAB script.

2.10. Zeta-potential measurement

The zeta-potential of the material was measured with a Malvern Zetasizer Nano ZS with folded capillary zeta cell (DTS1070, Malvern). Samples for measurement included AlgiMA 0.4%(w/v), ChiMA 0.4%(w/v) and GelMA 2%(w/v) solutions in DPBS. Lipofectamine3000 and AAV-2 samples were diluted by 100x with DPBS for measurement.

2.11. Release profile set-up

Release profile studies were performed in 1.5 mL Eppendorf tubes incubated in a 37 °C shaker at 100 rpm. 3 slab scaffolds were pooled into 1 tube. For Lipo@ChiMA, the slabs were incubated in 400 μL DPBS, and for the rest of the conditions, the slabs were incubated in 1000 μL DPBS. At designated time points, 20 μL of the DPBS was collected from each test tube at the top of the liquid, and 20 μL of fresh DPBS was added back to the tube. The cumulative release of the gene vectors at each time point was calculated accordingly and normalized to the total input.

2.12. Quantification of Lipofectamine3000 and AAV-2 release

Concentrations of Lipofectaime3000 and AAV-2 in the release samples were quantified by the GFP copies with quantitative polymerase chain reaction (qPCR) using a Quantstudio 3 system (Thermofisher). GFP primer (Forward: CGAAGGCTACGTCCAGGAGC; Reverse: CGATGTTGTGGCGGATCTTG) was purchased from Integrated DNA Technologies Inc. and reconstituted with UltraPure DNase/RNase-Free water (Cat. # 10977015, Invitrogen). The reaction was conducted with Luna Universal qPCR Master Mix (Cat. #3003, New England Biolabs Inc.). Lipofectamine3000 samples were directly quantified, while AAV-2 samples were purified through an AAV titer procedure. Briefly, the samples were incubated with DNase I (Cat. #M0303, New England Biolabs Inc.) at 37 °C for 15 min, 95 °C for 10 min, and cooled down to 4 °C, followed by incubation with Proteinase K (Cat. #P8107, New England Biolabs Inc.) at 37 °C for 15 min followed by 95 °C for 10 min. Both reactions were conducted in DNase I reaction buffer (Cat. #B0303, New England Biolabs Inc.). The samples were cooled down to 4 °C prior to proceeding to qPCR.

2.13. Cell culture, seeding and scaffold co-incubation

293T cells were obtained from ATCC and maintained in Dulbecco's Modified Eagle Medium (DMEM, Cat. #11965092, Gibco) with 10% fetal bovine serum (FBS, Cat. # 16000044, Gibco) in a CO_2 incubator at 37 °C. For functionality test, 20,000 cells were seeded in each well of a 12-well plate, and co-incubated at their normal culture condition with 5 slab scaffolds which were scraped from the coverslip confined in a cell insert (Cat. # 9310402, Sterlitech). The cell inserts were removed from the plates at designated time points, leaving the cell continue to culture.

2.14. Microscopic investigation and image analysis

24 h after co-incubation with AAV-2 scaffolds and 72 h after co-incubation with Lipofectamine3000 scaffolds, the cells were imaged for brightfield and green fluorescence with a Leica DMI 6000B fluorescent microscope. The cell area in brightfield and GFP positive area were measured with Image J [22] with the wand tool.

2.15. GFP assay

Quantification of green fluorescence protein was performed adapting a previously reported protocol [23]. Cells were lysed with a cell culture lysis buffer (Cat. #E1531, Promega) which is compatible with protein-based assays. The lysate was directly measured with a Tecan Infinite 200 Pro plate reader at 484/510 nm. To eliminate the variation due to difference in cell number in each well, a cell viability assay was

conducted prior to lysis with Cell Counting Kit – 8 (CCK-8, Cat. #K1018, ApexBio).

2.16. Statistical analysis

The data were presented as mean ± standard deviation (SD) with the experiments performed in triplicate. The analysis was performed with GraphPad Prism (Version 9.4.1). One-way analysis of variance (ANOVA) was used to analyze the variance of column data. Two-way ANOVA was used to analyze the release profile data. Pairwise comparison was performed using *t*-test. Difference with $P < 0.05$ was considered significant.

3. Results and discussion

3.1. Synthesis of the biomaterials

AlgiMA, GelMA, and ChiMA were successfully synthesized using established methods. AlgiMA was synthesized through a condensation reaction between the carboxyl groups in the alginate backbone and AEMA (Fig. 1Ai), while GelMA and ChiMA were synthesized via an amidation reaction between their primary amine groups and methacrylic anhydride (Fig. 1Ai, Aii). Following synthesis and purification, the materials were dissolved in DPBS, a saline buffer with physiologically relevant pH values. Photopolymerization during DLP printing was successfully induced by adding LAP, a biocompatible photoinitiator, to the solution.

All the three materials were compatible with the DLP printing system for high-resolution 3D printing of a customized pattern (Fig. 1B). The user-defined renal medulla mimicking pattern with the finest feature on the micron-scale are printed with all the three materials (Fig. 1B). Fluorescent beads were blended in the materials to facilitate the imaging of the transparent prints. To demonstrate the printing resolution of the DLP printing system and the biomaterial used, an array of simple geometries (circles, squares and lines) was printed, and the specimen sizes were compared with the computer design (Figs. S1A–C). Overall, the specimen sizes were systematically and slightly bigger than the designed size due to light scattering and free radical diffusion, which is a common problem in light-based printing. For more accurate size control, neural network-generated masks could be used to control the light exposure dose and compensate the light scattering effect [24]. A series of squares with descending sizes were also printed to showcase the smallest feature achievable with the fabrication platform (Fig. S1D). As summarized in Table S1, tens of microns were achievable with all the three materials. Squares with a side length as small as 14.40 μm, 18.97 μm and 20.95 μm were printed with AlgiMA, ChiMA and GelMA, respectively, with increased light exposure, despite that it gave rise to the over-polymerization problem of bigger features. Moreover, scaffolds printed with all the three materials showed a typical porous surface morphology of hydrogel materials after lyophilization (Fig. S2).

The net charge that each material carried in DPBS was verified by the zeta-potential measured via dynamic light scattering. As shown in Fig. 1D, the three materials showed distinct zeta-potentials when they were dissolved in DPBS. The zeta-potential of AlgiMA and ChiMA were −31.37 ± 1.57 mV and 7.9± 0.20 mV, respectively, consistent to their previously reported isoelectric points (pI) of 5.4 (alginate [25]) and 7.0–9.0 (chitosan [26]). Type A gelatin, which was the ingredient for GelMA synthesis in this study, typically had an isoelectric point of 9.0. The methacrylation reaction significantly consumed the amino groups of arginine in the gelatin backbone, leading to a lower pI of the GelMA product [27]. Here, the zeta-potential of GelMA solution in DPBS was −3.51 ± 0.50 mV as measured, which is close to zero and distinct from that of AlgiMA and ChiMA. Therefore, the three materials were employed as mock platforms with specific net charges to study the electrostatic adsorption, ion exchange or diffusion dominated release of the gene vectors.

The porosity and the stiffness of the photopolymerized materials were dominated by the degree of methacrylate substitution of the polymer [28], while alginate and chitosan have more active sites for methacrylation than gelatin. Therefore, the concentration of each material for DLP printing was adjusted to a value where their compression moduli were comparable. As shown in Fig. 1E, the Young's modulus of AlgiMA, GelMA and ChiMA was 2.52 ± 0.28 kPa, 2.79± 0.14 kPa and 3.06± 0.92 kPa, respectively at concentrations of 2.5%(w/v) for AlgiMA, 5%(w/v) for GelMA, and 2.5%(w/v) for ChiMA. With the Young's modulus controlled, the porosity and thereby the diffusion coefficients of the materials would only have negligible impact on release kinetics.

3.2. Release mechanism of the gene delivery cargos in different materials

AAV is a virus with single strand DNA. It has become one of the most preferred gene delivery vectors due to its simple genome, relatively low immunogenicity, and high and robust transduction efficiency [29]. Despite its success in reaching Phase III clinical trial for both hemophilia A and B as of 2020, AAV mediated gene therapy has been challenged by the instability of the vector in the nucleus of the targeted cells [30]. Therefore, encapsulation of AAV in scaffolds could potentially protect the vectors from degradation while being administered for local delivery [31].

AAV-2 features a positively charged heparin binding motif [32,33] which mediates its binding and infection, while the overall surface electrostatic potential is close to zero (Fig. S3) [34]. Here, AAV-2 is employed as the representative of the positive gene delivery cargo. As shown in Fig. 2A, AAV@GelMA showed a zero-order release with a zero-order constant (K) of 3.040 ($R^2 = 0.9908$), while AAV@ChiMA had a much higher K of 5.8587 ($R^2 = 0.9653$). AAV@AlgiMA showed a slight release over the investigation period of 14 days, showing a cumulative release of 0.39 ± 0.28% on day1, which increased to 4.24± 2.70% on day 7 and 4.61± 3.28% on day 14. In contrast, the cumulative release of AAV@ChiMA reached 56.35± 23.23% on day 7 and 70.90± 27.35% on day 14, while AAV@GelMA reached 21.80± 5.88% on day 7 and 45.53± 28.20% on day 14.

These results correspond to our hypothesis that electrostatic adsorption could substantially sustain the diffusion process of the gene delivery cargoes (AAV@AlgiMA vs. AAV@GelMA), while the elution of the cargoes was significantly accelerated when the substrate charge became the opposite (AAV@ChiMA vs. AAV@AlgiMA), which is partially driven by electrostatic repulsion (AAV@ChiMA vs. AAV@GelMA), as summarized in Fig. 2C.

Despite the high transduction efficiency and success in therapy development of the viral vectors, non-viral vectors have been essentially preferred due to their superior biosafety [35]. As a typical synthetic delivery vector, liposomes have been extensively exploited for *in vitro* and *in vivo* transfection. Here, Lipofectamine 3000, a commercially available liposomal gene vector was used for further release profile studies for the DLP-printed gene delivery scaffolds. Although composed of cationic lipid, the zeta potential of the freshly prepared lipofectamine is slightly negative (Fig. S3) [36], potentially due to the DNA plasmid attached on the outer surface of the cargo. Therefore, lipofectamine 3000 is chosen as the negative representative. In contrast to the AAV-2 release profile in the three materials, lipofectamine 3000 showed fastest release in AlgiMA ($K = 1.903$, $R^2 = 0.9945$) and slowest release in ChiMA, with a negligible cumulative release until day 14. On the other hand, Lipo@GelMA showed a moderate release with a K of 0.374 ($R^2 = 0.9388$) (Fig. 2B). These results conversely aligned with the AAV-2 release profile.

Collectively, the distinct profile raised by the electrostatic potential of the material validates the hypothesis of the potential of electrostatic adsorption in tailoring the release kinetics of the gene delivery cargoes as a supplement to the diffusion mechanism.

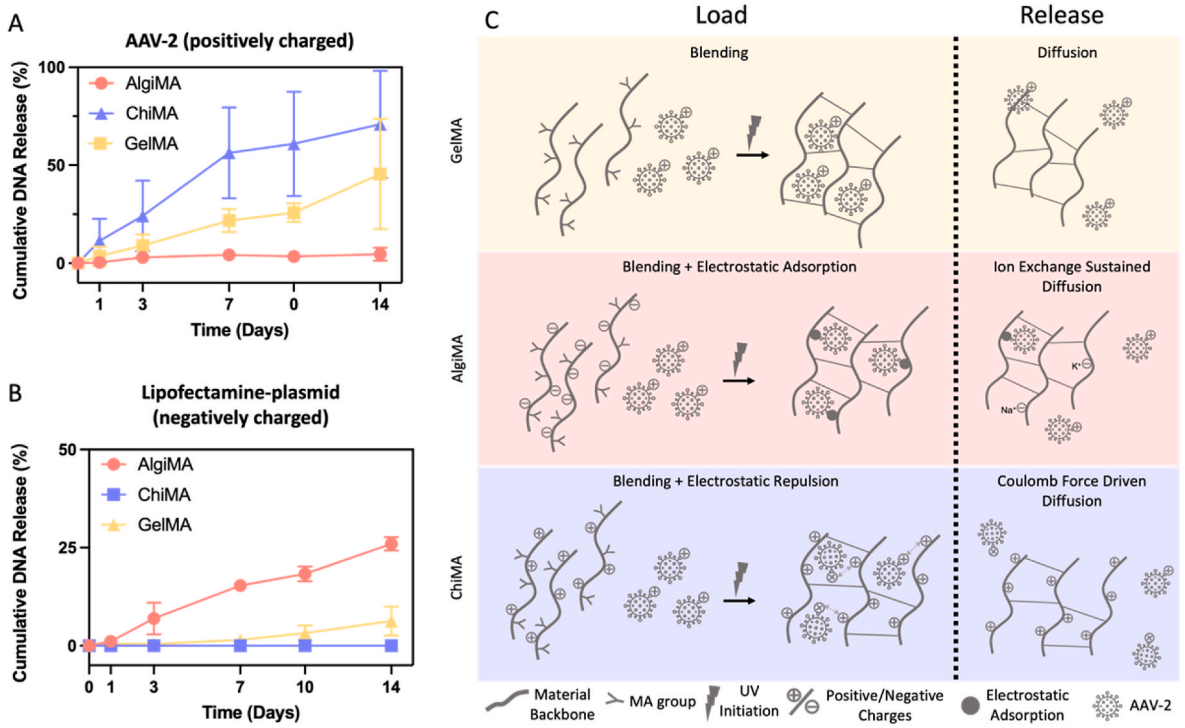

Fig. 2. Distinct release profile of AlgiMA, GelMA or ChiMA laden with A) AAV-2 (Material factor P = 0.0016**) and B) Lipofectamine3000 (Material factor P < 0.0001****); C) Illustration of the tunable cargo release mechanism with different combination of substrate and cargo charges.

3.3. Tunable release kinetics of the gene delivery cargos in different materials

Tailored release profile is prevalently desired in multiple applications of gene delivery, including therapeutic development, tissue regeneration, and manipulation of *in vitro* tissue. Based on the distinct release mechanisms of gene delivery cargos, we further investigated the potential of the system to provide a widened range of regulation in the release kinetics by adjusting the concentration of the polymer.

The sustained release of AAV from AlgiMA was mitigated by decreasing the concentration of AlgiMA while keeping all the other parameters consistent. Such precision control can be easily achieved in our DLP printing process. As shown in Fig. 3A, release of AAV from 2.5% AlgiMA reached a plateau at 3.5 ± 1.72% on day 7, while the cumulative

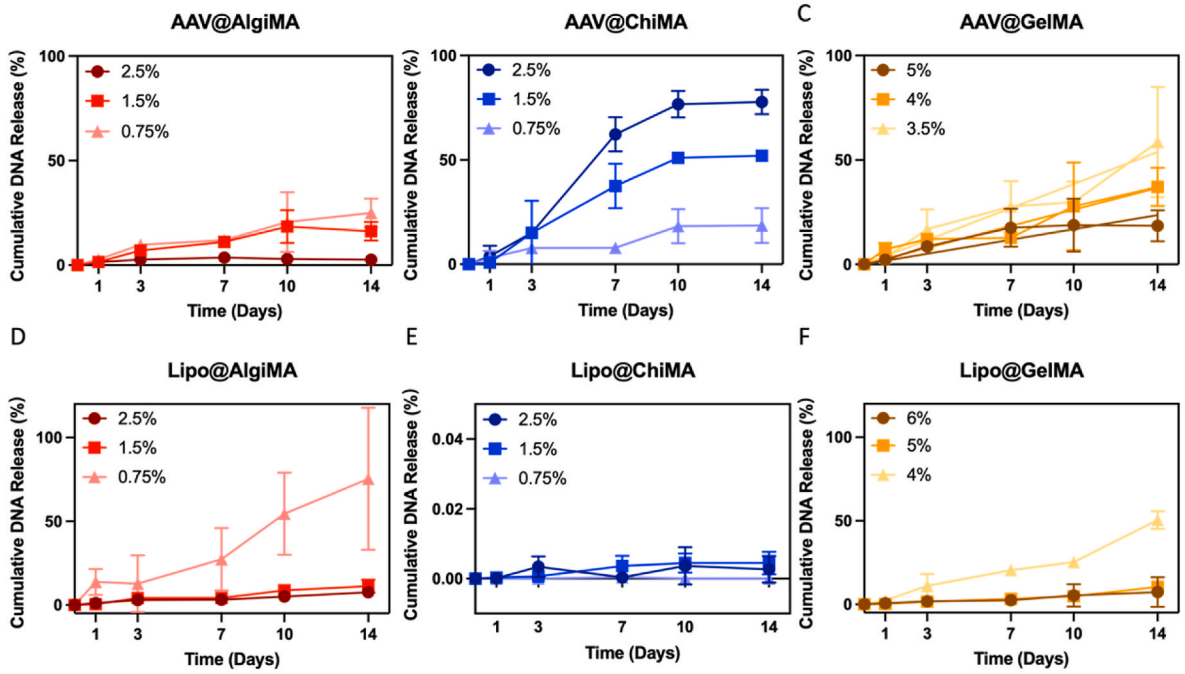

Fig. 3. Cumulative release profile of varied material concentration. A) AAV@AlgiMA (Concentration factor P = 0.0006***), B) AAV@ChiMA (Concentration factor P = 0.0015**), C) AAV@GelMA (Concentration factor P = 0.1837); D) Lipo@AlgiMA (Concentration factor P = 0.0627), E) Lipo@ChiMA (Concentration factor P = 0.3679), F) Lipo@GelMA (Concentration factor P = 0.0080**).

release elevated to 11.12± 1.46% and 11.93± 2.43% as observed in the parallel experiments with AlgiMA concentration set at 1.5% and 0.75%, respectively. As of day 14, the period of observation, with a cumulative AAV release of 16.18± 4.46% and 25.00± 6.98% from 1.5% to 0.75% AlgiMA. Two-way ANOVA identified the AlgiMA concentration as a significant source of variation between the groups ($P = 0.0006$), while GelMA concentration was nonsignificant (0.1837) despite the distinct K increase with the reducing material concentration (5%: 1.682, 4%: 2.620, 3.5%: 3.850), implying a shift in the release mechanism. Decreasing the concentration of AlgiMA reduced the negatively charged sites available for electrostatic adsorption of AAV while enlarging the pore size of the polymer network. As the sustained release of AAV from AlgiMA was dominated by the electrostatic adsorption and facilitated by diffusion, the retention was partially discharged with the decrease of AlgiMA concentration and diffusion became the predominant release mechanism.

Reversed results were observed for ChiMA. With the decrease in material concentration, the release rate of AAV reduced as the density of the positive charges was lower. When ChiMA concentration was reduced to 0.75%, 7.91 ± 2.77% and 18.52± 8.34% of AAV-2 was released as of day 7 and day 14, respectively, with a K of 1.472 ($R^2 = 0.9557$). This rate is substantially lower than that of the 2.5% ChiMA ($K = 6.594$, $R^2 = 0.9615$), but the overall trend was similar to 5% GelMA, where the diffusion was the major mechanism to mediate release. The release was further accelerated in the GelMA scaffold when the material concentration was decreased to 4% and 3.5%, as shown in Fig. 3C.

In summary, tuning the concentration of the polymer effectively adjusted the release mechanism, and thereby the release kinetics of AAV. The results were slightly different for the case of Lipofectamine. Unlike AAV@ChiMA where the cargo and the substrate had opposite charges, Lipo@AlgiMA showed an increased release rate when the material concentration was reduced, possibly due to the different charge density and material interaction between the two combinations. On the other hand, the release profile of Lipo@ChiMA of the three different concentrations were difficult to differentiate due to the low amount of cumulative release and the limitation of the quantification technique. Overall, these results suggest a widened tunable kinetic range of the gene delivery system which could potentially facilitate the development of point-of-care gene therapies with multi-gene and multi-phase releases.

3.4. Functional validation of the DLP-printed gene delivery system

293T cell line was used to evaluate the efficacy of the DLP-printed gene delivery system. The cells were seeded in a 12 well-plate and co-incubated with the green fluorescence protein (GFP) gene delivery cargo laden hydrogel lodged in a cell insert under normal growth condition. After designated co-incubation time, the cell insert was removed, and the cell was cultured until designated time points for characterization. The GFP expression was first briefly investigated by an inverted fluorescence microscope, and then lysed for quantification with a plate reader-based GFP assay.

As shown in Fig. 4A, the ratio of GFP-positive cells was substantially higher with the GFP signal stronger in the AAV@ChiMA treated cells after 2 h of scaffold co-incubation followed by 24 h of normal incubation, indicating the functional integrity of AAV was maintained after the DLP printing and cell co-incubation process. As a contrast, AAV@GelMA treated group had a moderate GFP-positive ratio with a lower signal intensity, while very few cells in the AAV@AlgiMA treated group expressed detectable GFP fluorescence. The results were further summarized in Fig. 4B, in which the ratio of GFP positive area in the overall cell covered area was measured and calculated with ImageJ.

To further quantify the efficacy of GFP transfection, the cells were then lysed with a cell lysis buffer which is compatible with protein assays for GFP assay. Before lysis, CCK-8 assay was performed to determine the overall cell viability in each well to eliminate the contribution of varied cell autofluorescence to the GFP signal due to varied cell number across the samples. As shown in Fig. 4C, AAV@ChiMA treated cells had an average GFP intensity of 6737 ± 514.73, significantly higher than that of AAV@GelMA (5052.17± 738.86) ($P < 0.01$), while the GFP intensity of AAV@AlgiMA treated cells was only 4897± 358.65, close to that of the non-treatment cells (4682.67± 323.02). Similar

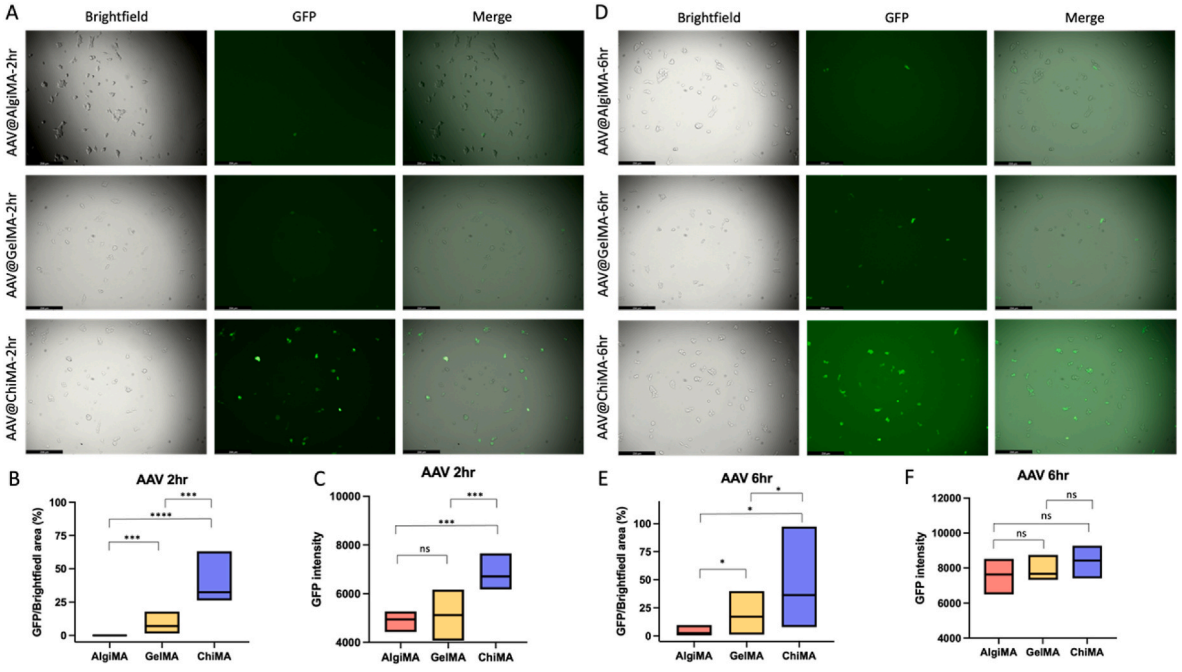

Fig. 4. GFP transfection results of AAV-laden scaffolds on 293T cells. Microscopic images of cells after co-incubation with AAV-laden scaffolds for 2 h (A) and 6 h (D) (scale bar = 256 μm); Ratio of GFP positive cell area versus brightfield cell area summarized from the microscopic images after co-incubation for 2 h (B, one-way ANOVA $P < 0.0001$****) and 6 h (E, one-way ANOVA $P = 0.0136$*); GFP intensity of the cells lysates measured at 484/510 nm after co-incubation for 2 h (C, one-way ANOVA $P = 0.0002$***) and 6 h (F, one-way ANOVA $P = 0.5284$). Data presented as mean, maximum value and minimum value.

results with an overall elevated tranexpression level were observed with the cells co-incubated with the scaffolds for 6 h and then incubated for 24 h under normal growth conditions (Fig. 4D, E, F). After co-incubation with the scaffolds for both 2 h and 6 h, all the cells showed a typical epithelial like morphology, as shown in Fig. S4.

The GFP intensity of the AAV@AlgiMA, AAV@GelMA or AAV@-ChiMA treated cells was consistent with the microscopic observations as well as the release profile results as discussed in 2.2. This result suggested that tuning the release profile of the DLP-printed AAV delivery system could effectively regulate the transfection kinetics of the system accordingly, implying the potential of the system to be translated to real-life research or therapeutic applications.

In the case of Lipofectamine, the cell transfection efficacy was significantly compromised in the DLP printed systems with all the three materials, showing an overall extremely low GFP intensity (Fig. S5). It was notable that the cells co-incubated with all the scaffolds showed the typical epithelial morphology of 293T, only aggregating at regions of very high confluency, while Lipofectamine 3000 positive control had a morphology shift into distinct aggregations even at low density (Fig. S6). Therefore, the lack of transfection efficacy is possibly caused by the structural incompatibility between our DLP-printed hydrogel scaffold system and the Lipofectamine 3000 reagent. Controlled and tunable transfection is highly potent to be achievable with appropriate modification and optimization on the liposome construction as well as the bioink for DLP printing.

4. Conclusion

We have established a DLP-based bioprinting platform to fabricate hydrogel scaffolds for gene delivery. This platform was validated with 2 gene delivery cargos, Lipofectamine 3000 and AAV-2, and 3 biomaterials, GelMA, AlgiMA and ChiMA. By choosing the material and tuning the material composition, release kinetics of the gene delivery cargoes in the DLP printing system can be tailored through the combination of diffusion and ion exchange mechanism and the transfection kinetics of AAV-2 could be regulated by tailoring the release kinetics. By appropriate modification and optimization of the cargo, the system is potentially compatible with further gene delivery cargoes, such as liposomal vectors, as well as other therapeutics, such as small molecules, growth factors, and cells. Furthermore, multiphase release of multi-substances could be achieved by multi-layer and multi-material printing, holding a high potential for the development of a synergistic and personalized treatment.

CRediT authorship contribution statement

Yi Xiang: Conceptualization, Methodology, Validation, Formal analysis, Investigation, Writing – original draft, Writing – review & editing, Visualization. **Zheng Zhong:** Conceptualization, Methodology, Validation, Writing – review & editing. **Emmie J. Yao:** Methodology, Validation, Investigation. **Wisarut Kiratitanaporn:** Methodology, Validation, Investigation. **Malleeka T. Suy:** Investigation, Writing – review & editing. **Shaochen Chen:** Conceptualization, Writing – original draft, Writing – review & editing, Resources, Supervision, Project administration, Funding acquisition.

Declaration of competing interest

The authors declare that they have no known competing financial interests or personal relationships that could have appeared to influence the work reported in this paper.

Data availability

Data will be made available on request.

Acknowledgements

This study was funded in part by grants from the US National Science Foundation (1937653, 2135720 and 2223669) and the National Institutes of Health (ES034455). The authors would like to acknowledge Ms. Audrey H. Lee's contribution in data analysis in the functional validation experiments.

Appendix A. Supplementary data

Supplementary data to this article can be found online at https://doi.org/10.1016/j.bprint.2023.e00270.

References

[1] T.M. Belete, The current status of gene therapy for the treatment of cancer, Biologics 15 (2021) 67–77, https://doi.org/10.2147/BTT.S302095.
[2] C.E. Dunbar, K.A. High, J.K. Joung, D.B. Kohn, K. Ozawa, M. Sadelain, Gene therapy comes of age, Science (1979), https://doi.org/10.1126/science.aan4672, 2018;359.
[3] M. Cucchiarini, H. Madry, Biomaterial-guided delivery of gene vectors for targeted articular cartilage repair, Nat. Rev. Rheumatol. 15 (2019) 18–29, https://doi.org/10.1038/s41584-018-0125-2.
[4] H. Storrie, D.J. Mooney, Sustained delivery of plasmid DNA from polymeric scaffolds for tissue engineering, Adv. Drug Deliv. Rev. 58 (2006) 500–514, https://doi.org/10.1016/j.addr.2006.03.004.
[5] T.-C. Ho, H. Sung Kim, Y. Chen, Y. Li, M.W. LaMere, C. Chen, et al., Scaffold-mediated CRISPR-Cas9 delivery system for acute myeloid leukemia therapy, Sci. Adv. 7 (21) (2021), eabg3217, https://doi.org/10.1126/sciadv.abg3217.
[6] S. Xiao, Q. Peng, Y. Yang, Y. Tao, Y. Zhou, W. Xu, et al., Preparation of [Amine-Terminated generation 5 poly(amidoamine)]- graft-Poly(lactic- co-glycolic acid) electrospun nanofibrous mats for scaffold-mediated gene transfection, ACS Appl. Bio Mater. 3 (2020) 346–357, https://doi.org/10.1021/acsabm.9b00848.
[7] C. Yu, J. Schimelman, P. Wang, K.L. Miller, X. Ma, S. You, et al., Photopolymerizable biomaterials and light-based 3D printing strategies for biomedical applications, Chem. Rev. 120 (2020) 10695–10743, https://doi.org/10.1021/acs.chemrev.9b00810.
[8] M. Qu, H.J. Kim, X. Zhou, C. Wang, X. Jiang, J. Zhu, et al., Biodegradable microneedle patch for transdermal gene delivery, Nanoscale 12 (2020) 16724–16729, https://doi.org/10.1039/d0nr02759f.
[9] Y. Lei, M. Rahim, Q. Ng, T. Segura, Hyaluronic acid and fibrin hydrogels with concentrated DNA/PEI polyplexes for local gene delivery, J. Contr. Release 153 (2011) 255–261, https://doi.org/10.1016/j.jconrel.2011.01.028.
[10] D. Chuan, T. Jin, R. Fan, L. Zhou, G. Guo, Chitosan for gene delivery: methods for improvement and applications, Adv. Colloid Interface Sci. 268 (2019) 25–38, https://doi.org/10.1016/j.cis.2019.03.007.
[11] J.L. Madrigal, S. Shams, R.S. Stilhano, E.A. Silva, Characterizing the encapsulation and release of lentivectors and adeno-associated vectors from degradable alginate hydrogels, Biomater. Sci. 7 (2019) 645–656, https://doi.org/10.1039/c8bm01218k.
[12] P. Soman, B.T.D. Tobe, J.W. Lee, A.M. Winquist, I. Singec, K.S. Vecchio, et al., Three-dimensional scaffolding to investigate neuronal derivatives of human embryonic stem cells, Biomed. Microdevices 14 (2012) 829–838, https://doi.org/10.1007/s10544-012-9662-7.
[13] W. Zhu, K.R. Tringale, S.A. Woller, S. You, S. Johnson, H. Shen, et al., Rapid continuous 3D printing of customizable peripheral nerve guidance conduits, Mater. Today 21 (2018) 951–959, https://doi.org/10.1016/j.mattod.2018.04.001.
[14] Z. Zhong, X. Deng, P. Wang, C. Yu, W. Kiratitanaporn, X. Wu, et al., Rapid bioprinting of conjunctival stem cell micro-constructs for subconjunctival ocular injection, Biomaterials 267 (2021), https://doi.org/10.1016/j.biomaterials.2020.120462.
[15] A.S. Khalil, X. Yu, J.M. Umhoefer, C.S. Chamberlain, L.A. Wildenauer, G.M. Diarra, et al., Single-dose mRNA therapy via biomaterial-mediated sequestration of overexpressed proteins, Sci. Adv. 6 (27) (2020), eaba2422, https://doi.org/10.1126/sciadv.eaba2422.
[16] M.M. Pakulska, I.E. Donaghue, J.M. Obermeyer, A. Tuladhar, C.K. McLaughlin, T. N. Shendruk, et al., Encapsulation-free controlled release: electrostatic adsorption eliminates the need for protein encapsulation in PLGA nanoparticles, Sci. Adv. 2 (2016), https://doi.org/10.1126/sciadv.1600519.
[17] T. Kawai, K. Saito, W. Lee, Protein binding to polymer brush, based on ion-exchange, hydrophobic, and affinity interactions, J. Chromatogr., B: Anal. Technol. Biomed. Life Sci. 790 (2003) 131–142, https://doi.org/10.1016/S1570-0232(03)00090-4.
[18] H. Shirahama, B.H. Lee, L.P. Tan, N.J. Cho, Precise tuning of facile one-pot gelatin methacryloyl (GelMA) synthesis, Sci. Rep. 6 (2016), https://doi.org/10.1038/srep31036.
[19] S.I. Somo, K. Langert, C.Y. Yang, M.K. Vaicik, V. Ibarra, A.A. Appel, et al., Synthesis and evaluation of dual crosslinked alginate microbeads, Acta Biomater. 65 (2018) 53–65, https://doi.org/10.1016/j.actbio.2017.10.046.
[20] L.M.Y. Yu, K. Kazazian, M.S. Shoichet, Peptide surface modification of methacrylamide chitosan for neural tissue engineering applications, J. Biomed. Mater. Res. 82 (2007) 243–255, https://doi.org/10.1002/jbm.a.31069.

[21] B.D. Fairbanks, M.P. Schwartz, C.N. Bowman, K.S. Anseth, Photoinitiated polymerization of PEG-diacrylate with lithium phenyl-2,4,6-trimethylbenzoylphosphinate: polymerization rate and cytocompatibility, Biomaterials 30 (2009) 6702–6707, https://doi.org/10.1016/j.biomaterials.2009.08.055.

[22] C.A. Schneider, W.S. Rasband, K.W. Eliceiri, NIH Image to ImageJ: 25 years of image analysis, Nat. Methods 9 (2012) 671–675, https://doi.org/10.1038/nmeth.2089.

[23] M. Sharma, J.L. Tyagi, K.M. Poluri, Quantifying bacterial cell lysis using GFP based fluorimetric assay, Int. J. Biol. Macromol. 138 (2019) 881–889, https://doi.org/10.1016/j.ijbiomac.2019.07.172.

[24] S. You, J. Guan, J. Alido, H.H. Hwang, R. Yu, L. Kwe, et al., Mitigating scattering effects in light-based three-dimensional printing using machine learning, Journal of Manufacturing Science and Engineering, Transactions of the ASME 142 (2020), https://doi.org/10.1115/1.4046986.

[25] H.H. Paradies, D. Wagner, W.R. Fischer, Multicomponent diffusion of sodium alginate solutions with added salt. II. Charged vs. uncharged system, Berichte Der Bunsengesellschaft/Physical Chemistry Chemical Physics 100 (1996) 1299–1307, https://doi.org/10.1002/bbpc.19961000806.

[26] S. Khazaei, S.A. Mozaffari, F. Ebrahimi, Polyvinyl alcohol as a crucial omissible polymer to fabricate an impedimetric glucose biosensor based on hierarchical 3D-NPZnO/chitosan, Carbohydr. Polym. 266 (2021), 118105, https://doi.org/10.1016/j.carbpol.2021.118105.

[27] R.L. Alexa, H. Iovu, J. Ghitman, A. Serafim, C. Stavarache, M.M. Marin, et al., 3D-printed gelatin methacryloyl-based scaffolds with potential application in tissue engineering, Polymers 13 (2021) 1–17, https://doi.org/10.3390/polym13050727.

[28] M. Zhu, Y. Wang, G. Ferracci, J. Zheng, N.J. Cho, B.H. Lee, Gelatin methacryloyl and its hydrogels with an exceptional degree of controllability and batch-to-batch consistency, Sci. Rep. 9 (2019), https://doi.org/10.1038/s41598-019-42186-x.

[29] D. Duan, Systemic delivery of adeno-associated viral vectors, Curr Opin Virol 21 (2016) 16–25, https://doi.org/10.1016/j.coviro.2016.07.006.

[30] A. Cantore, L. Naldini, WFH State-of-the-art paper 2020: in vivo lentiviral vector gene therapy for haemophilia, Haemophilia 27 (2021) 122–125, https://doi.org/10.1111/hae.14056.

[31] S. Lee, J.S. Kim, H.S. Chu, G.W. Kim, J.I. Won, J.H. Jang, Electrospun nanofibrous scaffolds for controlled release of adeno-associated viral vectors, Acta Biomater. 7 (2011) 3868–3876, https://doi.org/10.1016/j.actbio.2011.06.035.

[32] A. Kern, K. Schmidt, C. Leder, O.J. Müller, C.E. Wobus, K. Bettinger, et al., Identification of a heparin-binding motif on adeno-associated virus type 2 capsids, J. Virol. 77 (2003) 11072–11081, https://doi.org/10.1128/jvi.77.20.11072-11081.2003.

[33] J. O'Donnell, K.A. Taylor, M.S. Chapman, Adeno-associated virus-2 and its primary cellular receptor-Cryo-EM structure of a heparin complex, Virology 385 (2009) 434–443, https://doi.org/10.1016/j.virol.2008.11.037.

[34] H.L. Hsu, A. Brown, A.B. Loveland, A. Lotun, M. Xu, L. Luo, et al., Structural characterization of a novel human adeno-associated virus capsid with neurotropic properties, Nat. Commun. 11 (2020), https://doi.org/10.1038/s41467-020-17047-1.

[35] H. Yin, R.L. Kanasty, A.A. Eltoukhy, A.J. Vegas, J.R. Dorkin, D.G. Anderson, Non-viral vectors for gene-based therapy, Nat. Rev. Genet. 15 (2014) 541–555, https://doi.org/10.1038/nrg3763.

[36] K.K. Son, D.H. Patel, D. Tkach, A. Park, Rapid report Cationic liposome and plasmid DNA complexes formed in serum-free medium under optimum transfection condition are negatively charged, Biochim. Biophys. Acta 1466 (1–2) (2000) 11–15, https://doi.org/10.1016/s0005-2736(00)00176-0.